

Supplementary Material for

Reproduction deep inside wood: a low O₂ and high CO₂ gas environment promotes egg
production by termite queens

Eisuke Tasaki, Yasuyuki Komagata, Tatsuya Inagaki, Kenji Matsuura*

*Laboratory of Insect Ecology, Graduate School of Agriculture, Kyoto University,
Kitashirakawa Oiwakecho, Kyoto 606-8502, JAPAN*

*Corresponding author

E mail address: kenjijpn@kais.kyoto-u.ac.jp

This file includes:

Text S1: Supplementary Material and Methods

Figure S1 and S2

Table S1 to S3

Other Supplementary Materials for this manuscript includes the following:

Dataset S1

Text S1: Supplementary Materials and Methods

Measurements of the O₂ and CO₂ concentrations in termite nests

To measure the O₂ and CO₂ concentrations in termite nests, six decayed pine logs were collected from secondary forests in Kyoto, Japan, during June and September 2016. Before cutting the logs, we determined the location of royal chambers in the logs based on the presence of royal guard soldiers or secondary queens with minimal structural disturbance [1]. We can roughly estimate the location of royal chamber area based on the distribution of eggs and 1st instar larvae. The soldiers guarding around royal chambers perform aggressive defence by rushing out and establish the final defence line unlike the soldiers in the foraging area [1], which provides solid clues for the location of royal chamber. Then, each log was cut into two or three parts so as to separate royal chamber area and foraging area. The decay class [2] and the volume of each piece of wood were shown in dataset S1. Five decayed pine logs without termites were also collected and recorded. To avoid the effect of nest disturbance, each part of wood was kept still in a moist chamber for over a week. Afterwards, a gas sample was collected from each part using the downward displacement of water in a water bath. Briefly, these logs were submerged in fresh water in 90-L water bath until air-bubbles do not occur even if the logs were repeatedly turned in the water. A clear plastic container filled with fresh water was located above the submerged logs and the rising air-bubbles were captured while dissecting the logs using knives in the water. We collected approximately 200 mL gas from each part of wood. A 100-mL gas sample was transferred from the container to a vacuum bag via the extraction syringe. Then, O₂ and

CO₂ concentrations of the gas samples were measured using an O₂ monitor (OxyMan OM25NP20, As One) and CO₂ monitor (GMT221, Vaisala), respectively.

After gas sampling, remaining part of the wood was carefully dissected to confirm royal chamber, i.e., the presence of reproductives. Each part of the termite-infested wood was categorised as either “foraging area” or “royal chamber area” based on the presence of kings and queens (figure 1a). O₂ and CO₂ concentrations outside the wood were also measured using O₂ monitor (OxyMan OM25NP20, As One) and CO₂ monitor (GCH-2018, Mother Tool), respectively, at experimental field sites in Kyoto University.

To determine the levels of both O₂ and CO₂ absorption during all handling procedures, we performed gas absorption analysis using reference gases (known O₂ and CO₂ gas mixtures). We demonstrated that only CO₂ gas concentrations were significantly different between before and after the gas handling (paired *t*-test, $t = 6.836$, $df = 11$, $p < 0.001$; figure S1). Therefore, the values of CO₂ gas concentrations of wood samples were calculated using the calibration curve yielded the equation $y = 0.458x$ ($r^2 = 0.7801$) (dataset S1).

figure S1

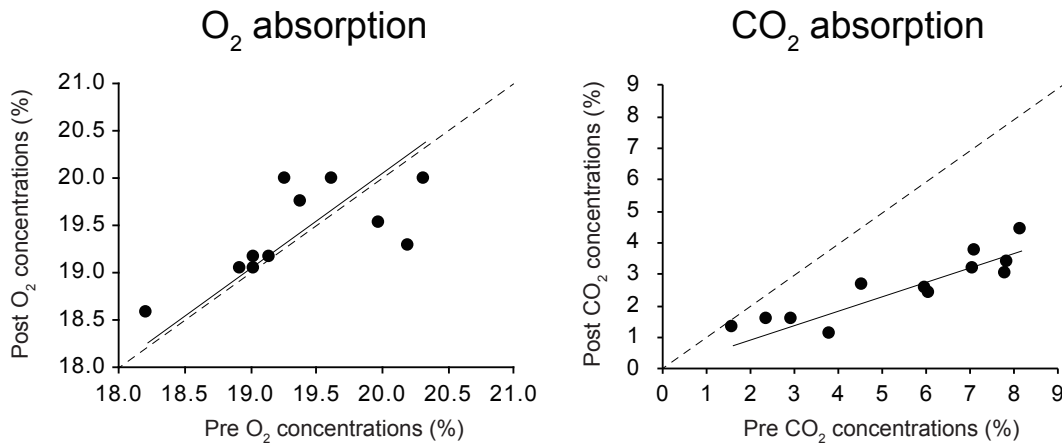


Figure S1. O₂ and CO₂ absorption in water during all handling procedures. Pre O₂ and CO₂ concentrations (x axis) show the reference gases' concentrations before the handling (%). Post O₂ and CO₂ concentrations (y axis) show these gas concentrations after the handling (%). Solid and broken lines indicate linear regression and $y = x$ (no-absorption in water), respectively.

Effect of gas condition on egg production

Three colonies of the termite *R. speratus* were collected from secondary forests in Japan, in August 2017 (colony A and B) and July 2019 (colony C). The only colony C had been kept under laboratory conditions for approximately five months until this experiment. All of the colonies had a primary king and queens (all were nymphoid neotenic). Queen body weight was significantly greater in colony A ($6.31 \pm 0.071\text{SE}$ mg) than in colony B (5.54 ± 0.079 ; likelihood ratio test, $\chi^2 = 14.04$, $df = 1$, $p < 0.001$) and colony C ($5.66 \pm 0.039\text{SE}$; likelihood ratio test, $\chi^2 = 19.30$, $df = 1$, $p < 0.001$; table S1). There was no difference of

queen body weight between colony B and C (likelihood ratio test, $\chi^2 = 0.38$, $df = 1$, $p = 0.162$; table S1). On the other hand, the highest body weights of total queens and a king were observed in colony C, followed in order by colony A and B (table S1).

Table S1. Weights and numbers of kings and queens

Colony	*Caste	Number	Mean body weight (mg)	Total body weight (mg)
A	PK	1	4.78	-
A	SQ	72	6.31 ± 0.071SE	454.30
B	PK	1	3.80	-
B	SQ	35	5.54 ± 0.079SE	193.81
C	PK	1	5.05	-
C	SQ	121	5.66 ± 0.039SE	684.36

* PK: primary king, SQ: secondary queen

For each colony, we placed a queen together with 100 nestmate workers in a 35-mm Petri dish containing moist mixed sawdust. The queens were randomly chosen from each colony and measured in body weight (pre-body weight; dataset S1). There was not significant difference in mean pre-body weight of the queens between the treatments in each colony (likelihood ratio test, colony A: $\chi^2 = 0.168$, $df = 1$, $p = 0.238$; colony B: $\chi^2 = 0.485$, $df = 1$, $p = 0.285$; colony C: $\chi^2 < 0.001$, $df = 1$, $p = 0.988$). The mixed sawdust was

made of brown rotten pine wood and cellulose powder in a 1:1 by-volume ratio. For the following tests, the Petri dishes were maintained for a month under ambient gas conditions (unregulated ambient gas conditions) or royal chamber gas conditions (15% O₂ and 5% CO₂) at 25°C in a multi-gas incubator (9000EX, Waken B Tech). Then, the number of eggs was counted with microscopic observation. Each queen was measured in body weight (post-body weight; dataset S1) and immediately frozen with liquid nitrogen and stored at -80°C until RNA extraction.

Expression of vitellogenin genes

The following seven homologs of *R. speratus* were obtained from the RNA sequencing database published in a previous study [3]: vitellogenin 1 (*RsVg1*; accession number: FX982957), vitellogenin 2 (*RsVg2*; accession number: FX982955), vitellogenin 3 (*RsVg3*; accession number: FX982958), glucose-6-phosphate 1-dehydrogenase (*RsG6PD*; accession number: FX983730), glyceraldehyde-3-phosphate dehydrogenase (*RsGAPDH*; accession number: FX983172) and beta-actin (*RsACT*; accession number: FX983744). We designed primer pairs for above four vitellogenin genes and three reference genes using Primer3 v1.1.4 [4](table S1). Two reference primers for NADH dehydrogenase subunit 5 (ND5) and elongation factor-1 alpha (EF1a) were referred to a previous study [5]. To select a best control gene in this study, the suitability of these reference genes of this species were evaluated by using NormFinder software [6]. Using RNeasy mini kit (Qiagen), total RNA was extracted individually from the whole bodies of queens that were prepared by the above method. cDNA was synthesized immediately from the RNA using a PrimeScript™

RT reagent kit (Takara) and preserved at -20°C for quantitative real-time PCR (qPCR) analysis. qPCR was performed using Applied Biosystems[®] StepOne[™] system (Thermo) with Power SYBR[™] Green PCR master mix (Thermo). All procedures were performed in accordance with each manufacturer's protocol. Relative expression levels were calculated using a typical $\Delta\Delta\text{Ct}$ method [7] (relative to “Ambient” in colony A). We performed four replicates for the experiment.

Furthermore, to confirm the identities of these vitellogenin genes *RsVg1*, *RsVg2*, and *RsVg3*, we performed multiple amino acid sequence alignments with CLUSTALW and conducted phylogenetic analyses using the molecular evolutionary genetics analysis software MEGA7 [8](figure S2). Gene evolutionary history was inferred using the maximum likelihood method based on the Le_Gascuel_2008 model [9], which is the best model based on the Bayesian information criterion. Vitellogenin homologs of termites (*R. speratus*, *Zootermopsis nevadensis*, *Cryptotermes secundus*) and of the other insects (Hymenoptera, Thysanoptera and Hemiptera) were analysed.

Table S2. Primer sequences

Target gene	Sequence (5'–3')	Amplicon (bp)
<i>RsVg1</i>	Forward; TCGACGTGATCGCAGAAAA	127
	Reverse; GAAGAAGAGGAGGAAGAAGAAGAGG	
<i>RsVg2</i>	Forward; AAGACAACCAGGCACCCAAC	109
	Reverse; GCACGCCTTTTACCGTTTTC	

<i>RsVg3</i>	Forward; TGGAAACACCAGCCATGAAC Reverse; TTCCAATGCGCTCTACAACC	108
<i>RsND5</i>	Forward; GCTGGGGGGGTTATTCATTCCAT Reverse; GGCATACCACAAAGGGCAAAA	125
<i>RsEfla</i>	Forward; GGTGATGCGGCTATTGTTAACC Reverse; GTGGTGGGAATTCTGAGAAAGATT	73
<i>RsG6PD</i>	Forward; GCACTTTGTTCGTTCTGATGAGTT Reverse; TCACTACACACTTCATCTGCCTTCT	144
<i>RsGAPDH</i>	Forward; CCATAGAAAAGGCTTCTGCACATT Reverse; AACAAACAAACATTGGGGCATC	89
<i>RsACT</i>	Forward; AAATCGTGCGTGACATCAAA Reverse; GGAACAGAGCCTCAGGACAG	168

Phylogenetic analysis of vitellogenin homolog sequences

To confirm the identities of these vitellogenin genes *RsVg1*, *RsVg2*, and *RsVg3*, we performed multiple amino acid sequence alignments and conducted phylogenetic analyses (figure S2). Furthermore, analyses of protein families and domains were also performed using InterProScan in OmicsBox software v1.1.164 (table S3). All *RsVg1–3* sequences contain conserved domains of vitellogenin genes: vitellogenin lipid transport domain (Vitellogenin_N) and von-Willebrand factor type D domain (VWD).

figure S2

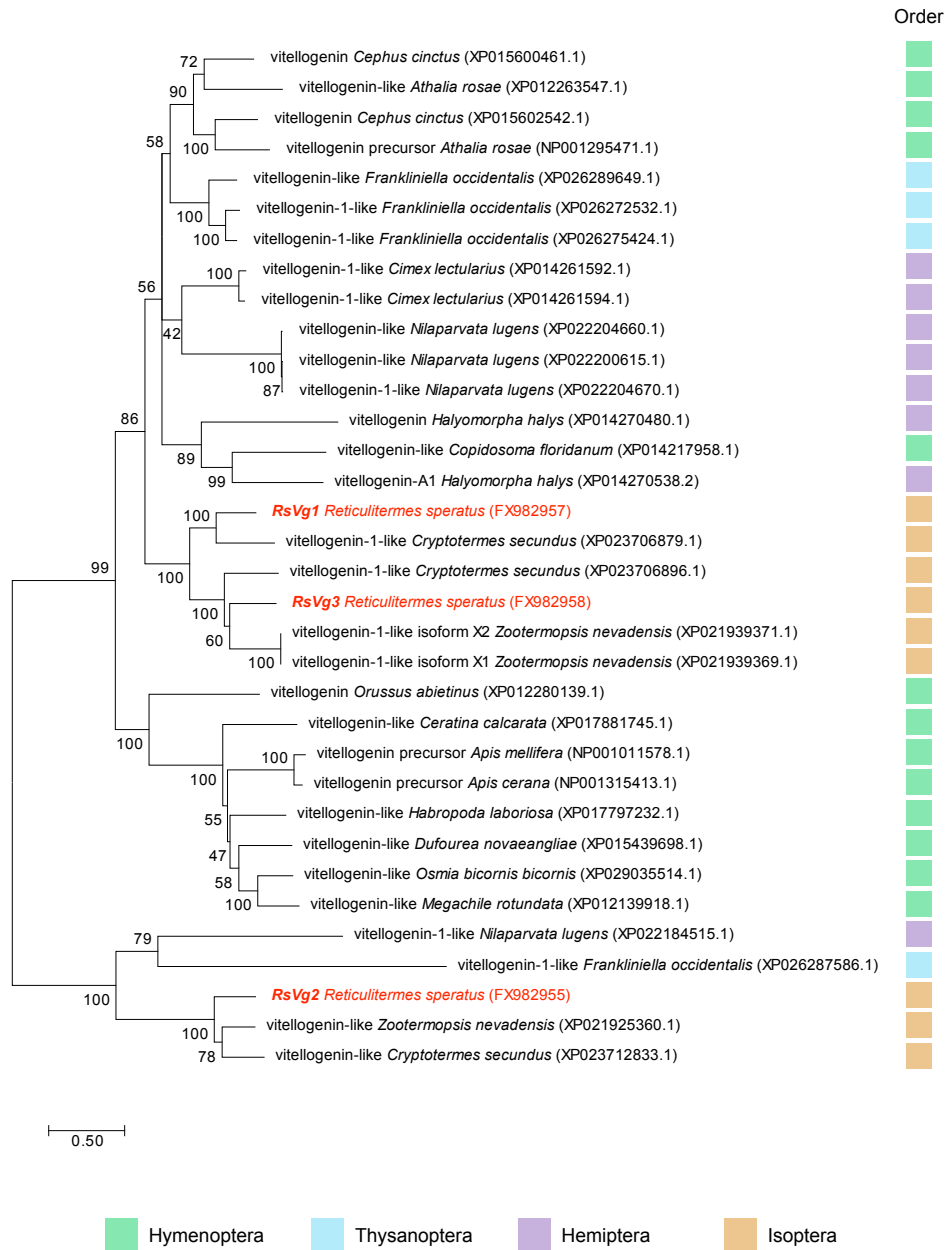


Figure S2. Maximum likelihood molecular phylogenetic tree of vitellogenin homolog sequences. The evolutionary history of vitellogenin homologs was inferred using the maximum likelihood method based on the Le_Gascuel_2008 model [9]. The tree with the highest log likelihood (-50245.84) is shown. The percentage of trees in which the associated taxa clustered together is shown above the branches. Initial tree(s) for the heuristic search were automatically obtained by applying Neighbour-Joining and BioNJ algorithms to a matrix of pairwise distances estimated using a JTT model, and then selecting the topology with a superior log likelihood value. A discrete gamma distribution was used to model the evolutionary rate differences among the sites (5 categories [+G, parameter = 2.3881]). The rate variation model allowed for some sites to be evolutionarily invariable ([+I], 0.38% sites). The tree is drawn to scale, with branch lengths measured in the number of substitutions per site. The analysis involved 34 amino acid sequences. All positions containing gaps and missing data were eliminated. There was a total of 933.

Table S3. Predicted *RsVg1*, *RsVg2*, and *RsVg3* families and domains

Gene name	AC	Type	Name	GO IDs	Library
<i>RsVg1</i>	IPR001747	Domain	Lipid transport protein, N-terminal	GO:0005319 GO:0006869	PF01347 (PFAM) PS51211 (PROSITE_PROFILES)
	IPR001846	Domain	von Willebrand factor, type D domain	-	PF00094 (PFAM) PS51233 (PROSITE_PROFILES)
	IPR011030	Homologous superfamily	Lipovitellin-phosvitin complex, superhelical domain	-	G3DSA:1.25.10.20 (GENE3D) SSF48431 (SUPERFAMILY)
	IPR015255	Domain	Vitellinogen, open beta-sheet	GO:0006869 GO:0005319	PF09172 (PFAM)
	IPR015816	Homologous superfamily	Vitellinogen, beta-sheet N-terminal	GO:0006869 GO:0005319	G3DSA:2.30.230.10 (GENE3D)
	IPR015819	Homologous superfamily	Lipid transport protein, beta-sheet shell	GO:0005319 GO:0006869	SSF56968 (SUPERFAMILY)
	no IPR	Homologous superfamily	Lipovitellin-phosvitin complex, superhelical domain	-	mobidb-lite (MOBIDB_LITE) PTHR23345 (PANTHER) PTHR23345:SF15 (PANTHER)
	no IPR	-	-	-	Coil (COILS)
<i>RsVg2</i>	IPR001747	Domain	Lipid transport protein, N-terminal	GO:0005319 GO:0006869	PF01347 (PFAM) PS51211 (PROSITE_PROFILES)
	IPR001846	Domain	von Willebrand factor, type D domain	-	PF00094 (PFAM) PS51233 (PROSITE_PROFILES)

	IPR011030	Homologous superfamily	Lipovitellin-phosvitin complex, superhelical domain	-	G3DSA:1.25.10.20 (GENE3D) SSF48431 (SUPERFAMILY)
	IPR015816	Homologous superfamily	Vitellinogen, beta-sheet N-terminal	GO:0006869 GO:0005319	G3DSA:2.30.230.10 (GENE3D)
	IPR015819	Homologous superfamily	Lipid transport protein, beta-sheet shell	GO:0005319 GO:0006869	SSF56968 (SUPERFAMILY)
	no IPR	Homologous superfamily	Vitellinogen, beta-sheet N-terminal	-	mobidb-lite (MOBIDB_LITE) PTHR23345 (PANTHER)
<i>RsVg3</i>	IPR001747	Domain	Lipid transport protein, N-terminal	GO:0005319 GO:0006869	PF01347 (PFAM) PS51211 (PROSITE_PROFILES)
	IPR001846	Domain	von Willebrand factor, type D domain	-	PF00094 (PFAM) PS51233 (PROSITE_PROFILES)
	IPR011030	Homologous superfamily	Lipovitellin-phosvitin complex, superhelical domain	-	G3DSA:1.25.10.20 (GENE3D) SSF48431 (SUPERFAMILY)
	IPR015255	Domain	Vitellinogen, open beta-sheet	GO:0006869 GO:0005319	PF09172 (PFAM)
	IPR015819	Homologous superfamily	Lipid transport protein, beta-sheet shell	GO:0005319 GO:0006869	SSF56968 (SUPERFAMILY)
	no IPR	Domain	Lipid transport protein, N-terminal	-	mobidb-lite (MOBIDB_LITE) PTHR23345:SF15 (PANTHER) PTHR23345 (PANTHER)

Statistical analysis

R software v3.3.2 was used for all statistical analyses. Unpaired *t*-test followed by *p* value correction using Holm's method [10] for multiple comparisons was performed on the different sets of gas condition data. We analysed data of the number of eggs laid, weights of queens and the relative expression levels of vitellogenin genes using generalised linear models (GLM) with Poisson and Gaussian distributions, respectively. We examined the effects of gas condition (GC) and colony of origin nested (C) as main effects and the interaction of GC × C. All data in results and graphs are presented as the mean ± standard error of mean (SEM). Differences were considered significant when the *p* value was < 0.05.

References

1. Yanagihara S, Suehiro W, Mitaka Y, Matsuura K. 2018 Age-based soldier polyethism: old termite soldiers take more risks than young soldiers. *Biol. Lett.* **14**. (doi:10.1098/rsbl.2018.0025)
2. Fukasawa Y. 2012 Effects of wood decomposer fungi on tree seedling establishment on coarse woody debris. *For. Ecol. Manage.* **266**, 232–238. (doi:10.1016/j.foreco.2011.11.027)
3. Mitaka Y, Kobayashi K, Mikheyev A, Tin MMY, Watanabe Y, Matsuura K. 2016 Caste-specific and sex-specific expression of chemoreceptor genes in a termite. *PLoS One* **11**, e0146125. (doi:10.1371/journal.pone.0146125)

4. Rozen S, Skaletsky H. 2000 Primer3 on the WWW for general users and for biologist programmers. *Methods Mol. Biol.* **132**, 365–386.
5. Hojo M, Toga K, Watanabe D, Yamamoto T, Maekawa K. 2011 High-level expression of the geranylgeranyl diphosphate synthase gene in the frontal gland of soldiers in *Reticulitermes speratus* (Isoptera: Rhinotermitidae). *Arch. Insect Biochem. Physiol.* **77**, 17–31. (doi:10.1002/arch.20415)
6. Andersen CL, Jensen JL, Ørntoft TF. 2004 Normalization of real-time quantitative reverse transcription-PCR data: A model-based variance estimation approach to identify genes suited for normalization, applied to bladder and colon cancer data sets. *Cancer Res.* **64**, 5245–5250. (doi:10.1158/0008-5472.CAN-04-0496)
7. Livak KJ, Schmittgen TD. 2001 Analysis of relative gene expression data using real-time quantitative PCR and the $2^{-\Delta\Delta CT}$ method. *Methods* **25**, 402–408. (doi:10.1006/meth.2001.1262)
8. Kumar S, Stecher G, Tamura K. 2016 MEGA7: molecular evolutionary genetics analysis version 7.0 for bigger datasets. *Mol. Biol. Evol.* **33**, 1870–1874. (doi:10.1093/molbev/msw054)
9. Le SQ, Gascuel O. 2008 An improved general amino acid replacement matrix. *Mol. Biol. Evol.* **25**, 1307–1320. (doi:10.1093/molbev/msn067)
10. Holm S. 1979 A simple sequentially rejective multiple test procedure. *Scand. J. Stat.* **6**, 65–70. (doi:10.2307/4615733)